

# An epitranscriptomic switch at the 5'-UTR controls genome selection during HIV-1 genomic RNA packaging

Camila Pereira-Montecinos<sup>1,2</sup>; Daniela Toro-Ascuy<sup>1,2#</sup>; Cecilia Rojas-Fuentes<sup>1,2</sup>; Sebastián Riquelme-Barrios<sup>1,2</sup>; Bárbara Rojas-Araya<sup>1,2</sup>; Francisco García-de-Gracia<sup>1,2</sup>; Paulina Aguilera-Cortés<sup>1,2</sup>; Catarina Ananías-Sáez<sup>1,2</sup>; Grégoire de Bisschop<sup>3</sup>; Jonás Chaniderman<sup>1</sup>; Mónica L. Acevedo<sup>1</sup>; Bruno Sargueil<sup>3</sup>; Fernando Valiente-Echeverría<sup>1,2</sup> and Ricardo Soto-Rifo<sup>1,2\*</sup>

<sup>1</sup> Laboratory of Molecular and Cellular Virology, Virology Program, Institute of Biomedical Sciences, Faculty of Medicine, Universidad de Chile, Santiago, Chile

<sup>2</sup> HIV/AIDS Workgroup (CHAIR), Faculty of Medicine, Universidad de Chile, Santiago, Chile

<sup>3</sup> CNRS UMR 8038, Laboratoire “Cibles Thérapeutiques et Conception de Médicaments” - CitCoM, Université Paris Descartes, 4 Avenue de l’Observatoire, 75270 Paris Cedex 06, France.

Fig. 1. Set. Diff. T. 1. (50.2.2050.60.60. E. 60)

Ricardo Soto-Ruiz. Tel. (50) 2 2978 08 09, Fax. (50) 2 2978 01 24,

tsotomio@uchile.cl

Universidad Autónoma de Chile, Santiago, Chile.

**Keywords:** N'-methyladenosine, HIV-1 genomic RNA, RNA Packaging, 5'-UTR, Gag

35 **ABSTRACT**

36 During retroviral replication, the full-length RNA serves both as mRNA and genomic RNA  
37 (gRNA). While the simple retrovirus MLV segregates its full-length RNA into two functional  
38 populations, the HIV-1 full-length RNA was proposed to exist as a single population used  
39 indistinctly for protein synthesis or packaging. However, the mechanisms by which the HIV-1  
40 Gag protein selects the two RNA molecules that will be packaged into nascent virions remain  
41 poorly understood. Here, we demonstrate that HIV-1 full-length RNA packaging is regulated  
42 through an epitranscriptomic switch requiring demethylation of two conserved adenosine  
43 residues present within the 5'-UTR. As such, while m<sup>6</sup>A deposition by METTL3/METTL14  
44 onto the full-length RNA was associated with increased Gag synthesis and reduced  
45 packaging, FTO-mediated demethylation was required for the incorporation of the full-length  
46 RNA into viral particles. Interestingly, HIV-1 Gag associates with the RNA demethylase FTO  
47 in the nucleus and drives full-length RNA demethylation. Finally, the specific inhibition of  
48 the FTO RNA demethylase activity suppressed HIV-1 full-length RNA packaging. Together,  
49 our data propose a novel epitranscriptomic mechanism allowing the selection of the full-  
50 length RNA molecules that will be used as viral genomes.

51

52

53

54

55

56

57

58

59

60

61

62

63

64

65

66

67

68

69 **INTRODUCTION**

70 Retroviral full-length RNA plays two key functions in the cytoplasm of infected cells. First, it  
71 is used as the mRNA template for the synthesis of Gag and Gag-Pol precursors and, second, it  
72 serves as the genomic RNA (gRNA) packaged into newly produced viral particles <sup>1-3</sup>. In  
73 contrast to the simple retrovirus murine leukemia virus (MLV), which was shown to segregate  
74 its full-length RNA into two functionally different populations serving as template for  
75 translation (mRNA) or packaging (gRNA), the HIV-1 and HIV-2 full-length RNA were  
76 proposed to exist as a single population acting indistinctly as mRNA and gRNA <sup>4-6</sup>. However  
77 and despite several years of efforts, there is still an important gap in our knowledge regarding  
78 the molecular mechanisms behind the selection of the full-length RNA molecules that will be  
79 incorporated into assembling viral particles.

80 The 5'-untranslated region (5'-UTR) present within the HIV-1 full-length RNA is the most  
81 conserved region of the viral genome and contains several high order structural motifs  
82 involved in different steps of the viral replication cycle from transcription, reverse  
83 transcription, splicing, translation to dimerization and packaging <sup>3, 7, 8</sup>. Since the full-length  
84 RNA serves both as mRNA and gRNA, translation and packaging are expected to be mutually  
85 exclusive events <sup>2</sup>. The Gag protein recognizes *cis*-acting RNA elements present at the 5'-  
86 UTR and the beginning of the Gag coding region and drives the selective incorporation of two  
87 copies of the gRNA into assembling viral particles. Indeed, there is accumulating evidence  
88 showing that dimerization and packaging of the HIV-1 full-length RNA are two tightly  
89 interconnected processes dependent on the Gag protein <sup>9-11</sup>. Structural and mutational  
90 analyses proposed that a conformational switch within the 5'-UTR regulates the transition  
91 from translation to dimerization and packaging *in vitro* <sup>12-15</sup>. In such models, the 5'-UTR  
92 alternates in conformations that occlude the dimerization initiation signal (DIS) or the Gag  
93 start codon thus, favoring translation or dimerization and packaging, respectively <sup>3, 8</sup>.  
94 However, chemical probing performed in cells and purified viral particles showed that a  
95 single structure, in which DIS is accessible for dimerization and packaging, predominates in  
96 these biological states <sup>16, 17</sup>. Moreover, the packaging prone structure does not interfere with  
97 full-length RNA translation suggesting that other factors rather than structural rearrangements  
98 are involved in the regulation of the cytoplasmic sorting of the HIV-1 full-length RNA <sup>18, 19</sup>.  
99 It was recently reported that the HIV-1 full-length RNA contains N<sup>6</sup>-methyladenosine (m<sup>6</sup>A)  
100 residues located at the 5'- and the 3'-UTR as well as at internal positions such as the Rev  
101 response element (RRE) <sup>20-22</sup>. Methylation of adenosines at the RRE and the 3'-UTR was  
102 shown to promote Gag synthesis by favoring nuclear export and/or the intracellular

103 accumulation of viral transcripts at late stages of the replication cycle<sup>20-23</sup>. However, it was  
104 also reported that the presence of m<sup>6</sup>A could also induce the degradation of the incoming  
105 gRNA early during infection<sup>22, 23</sup>. These controversial data prompted us to study whether  
106 m<sup>6</sup>A could serve as a mark that defines the functions of the HIV-1 full-length RNA as  
107 template for translation or packaging during viral replication.

108 Here, we show that methylation of two adenosine residues within the 5'-UTR by the  
109 METTL3/METLL14 complex inhibits full-length RNA packaging. m<sup>6</sup>A-seq analysis revealed  
110 that the full-length RNA present in purified viral particles lacks m<sup>6</sup>A at the 5'-UTR  
111 suggesting the existence of two populations that differ in their m<sup>6</sup>A patterns. Further  
112 bioinformatic analyses identified two highly conserved nucleotides A<sub>198</sub> and A<sub>242</sub> within the  
113 5'-UTR as the key residues involved in the m<sup>6</sup>A-mediated regulation of gRNA packaging. We  
114 also observed that the full-length RNA is a substrate for the RNA demethylase FTO, which  
115 together with Gag drives RNA demethylation to promote packaging. Finally, the  
116 pharmacological targeting of FTO activity resulted in impaired full-length RNA metabolism  
117 and a strong inhibition of packaging. Together, our data reveal a novel mechanism by which  
118 Gag selects the molecules of gRNA that will be used for packaging, which is regulated by an  
119 epitranscriptomic switch within the 5'-UTR.

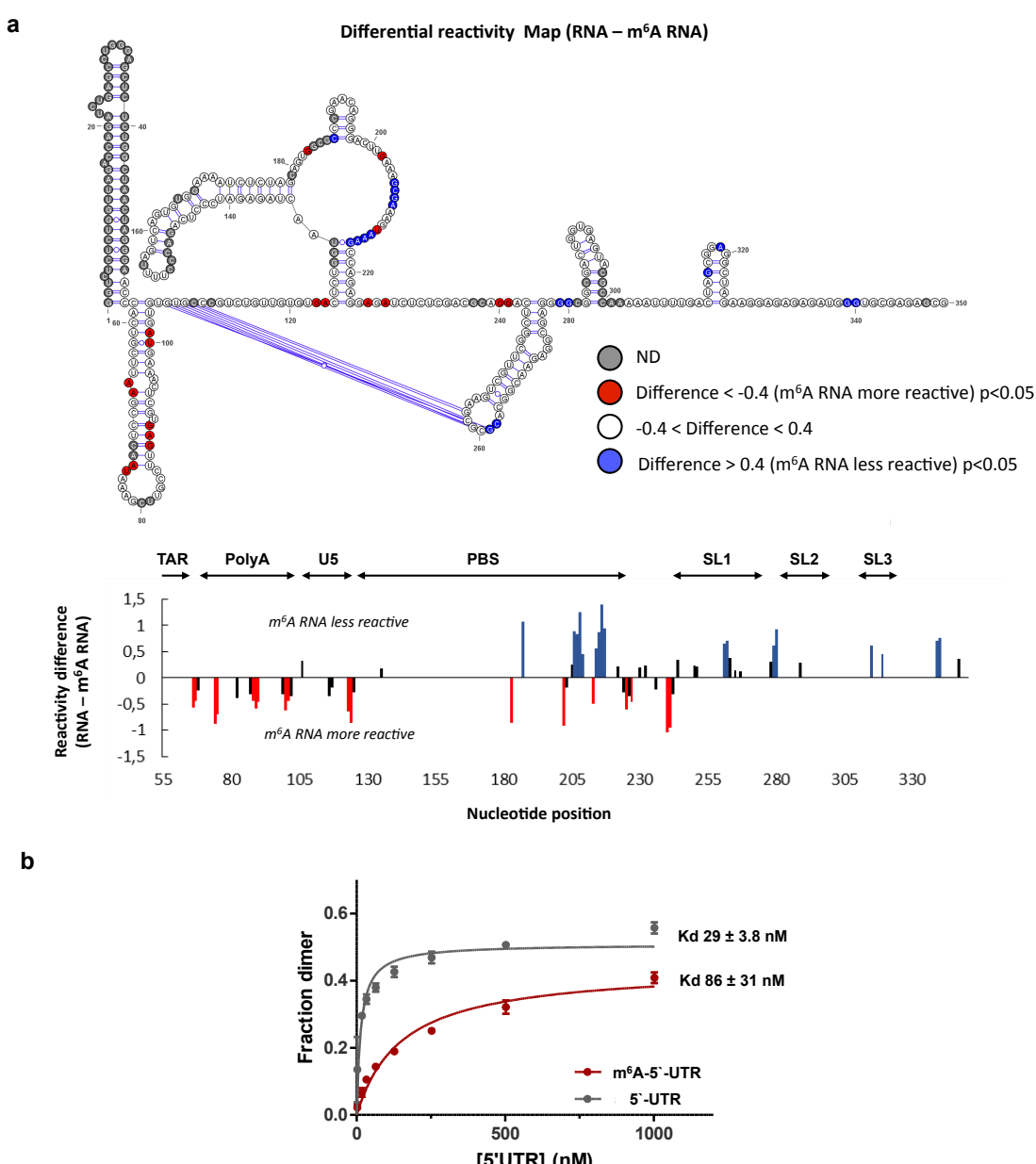
120

## 121 RESULTS

### 122 **The presence of m<sup>6</sup>A alters the *in vitro* folding and dimerization of the HIV-1 full-length 123 RNA 5'-UTR**

124 Since previous studies suggesting that a conformational switch of the 5'-UTR could regulate  
125 the ability of the HIV-1 full-length RNA to function as mRNA or gRNA have not considered  
126 the presence of RNA modifications such as m<sup>6</sup>A, we first sought to determine the impact of  
127 adenosine methylation on the folding of the 5'-UTR. As a first approach to study the impact  
128 of m<sup>6</sup>A on RNA structure, we generated an *in vitro*-transcribed 5'-UTR containing  
129 unmodified adenosines or a 5'-UTR in which all adenosines were replaced by m<sup>6</sup>A. Both  
130 m<sup>6</sup>A-5'-UTR and A-5'-UTR were submitted to 1M7 SHAPE analysis in parallel as described  
131 in Methods. Reactivity towards SHAPE reagents reveals the ribose flexibility, and as a  
132 consequence, the pairing status of each nucleotide. As such, higher reactivity of a given  
133 nucleotide means a higher probability to be in a single strand conformation. Comparative  
134 analysis of the SHAPE reactivity profiles indicates that the presence of m<sup>6</sup>A significantly  
135 alters the folding of the 5'-UTR (Fig. 1a and Supplementary Fig. 1a). The first interesting

136 observation from our SHAPE data is that we do not only observe a reactivity modification for  
 137 As or Us.



138  
 139 **Figure 1: The presence of m<sup>6</sup>A alters the *in vitro* folding and dimerization of the HIV-1 full-length RNA 5'-UTR. a,**  
 140 SHAPE reactivity differences between *in vitro* transcribed 5'-UTR RNA containing 0% m<sup>6</sup>A or 100% m<sup>6</sup>A plotted on the  
 141 secondary structure model of the HIV-1 full-length RNA 5'-UTR (upper panel). Nucleotides in red are significantly more  
 142 reactive with m<sup>6</sup>A whereas those in blues are significantly less reactive (p-value < 0.05 and reactivity difference > 0.4).  
 143 Nucleotides in white are of equivalent reactivity. Sites where the reactivity could not be determined are depicted in grey. The  
 144 histogram shows the reactivity difference between 0% m<sup>6</sup>A 5'-UTR and 100% m<sup>6</sup>A 5'-UTR (lower). Blue and red bars  
 145 highlight nucleotides with a significantly lower or higher reactivity in the 100% m<sup>6</sup>A RNA than in the 0% m<sup>6</sup>A RNA (p-  
 146 value < 0.05 and reactivity difference > 0.4), respectively. Significative differences that are below the threshold of 0.4 are  
 147 indicated in black. **b**, Fraction of dimers determined by electromobility shift assay for different concentrations of *in vitro*  
 148 transcribed 5'-UTR (1 μM, 0.5 μM, 0.25 μM, 127 nM, 65 nM, 33 nM, 18 nM, 2 nM) harboring either 0% of m<sup>6</sup>A (grey) or  
 149 100% of m<sup>6</sup>A (red) with the dissociation constants obtained from the data points (see Methods for details).

150 Moreover, although all adenosines were methylated in the m<sup>6</sup>A-5'-UTR RNA only local  
151 reactivity changes, often clustered, were observed suggesting that the presence of m<sup>6</sup>A  
152 influences the folding of specific domains or motifs within the 5'-UTR. The presence of m<sup>6</sup>A  
153 is predicted and has been observed to destabilize A-U pairings embedded in helical regions.  
154 This is mostly in agreement with the destabilizations (increase in reactivity) that are often  
155 observed for As, Us or in nucleotides in close proximity with proposed A-U base pairs. In  
156 particular, this could explain the reactivity enhancement within the poly-A stem, which is  
157 likely to be globally destabilized by m<sup>6</sup>A. However, none of the other nucleotides for which  
158 we observe a reactivity increase is involved or are close to A-U pairings and most of them are  
159 not even predicted to be base paired in most of the published models. In contrast, m<sup>6</sup>A has  
160 been shown to stabilize A-U pairings when preceded in 5' by a bulged nucleotide. This does  
161 not offer a rationale for any of the reactivity drop we observe which are mostly predicted to  
162 be in single strand regions thus, suggesting that m<sup>6</sup>A modulates a higher order structure  
163 and/or tertiary pairings yet to be identified. This prompted us to monitor dimerization of the  
164 5'-UTR and m<sup>6</sup>A-5'-UTR *in vitro*. We observed that the presence of m<sup>6</sup>A reduces but not  
165 abolish the efficiency of dimerization (Fig. 1b). The structure of the HIV-1 full-length RNA  
166 dimer is still poorly defined and a matter of debate, thus the dimerization deficiency observed  
167 does not provide a straightforward explanation for all the alterations of the SHAPE profile but  
168 could reveal unknown rearrangements.

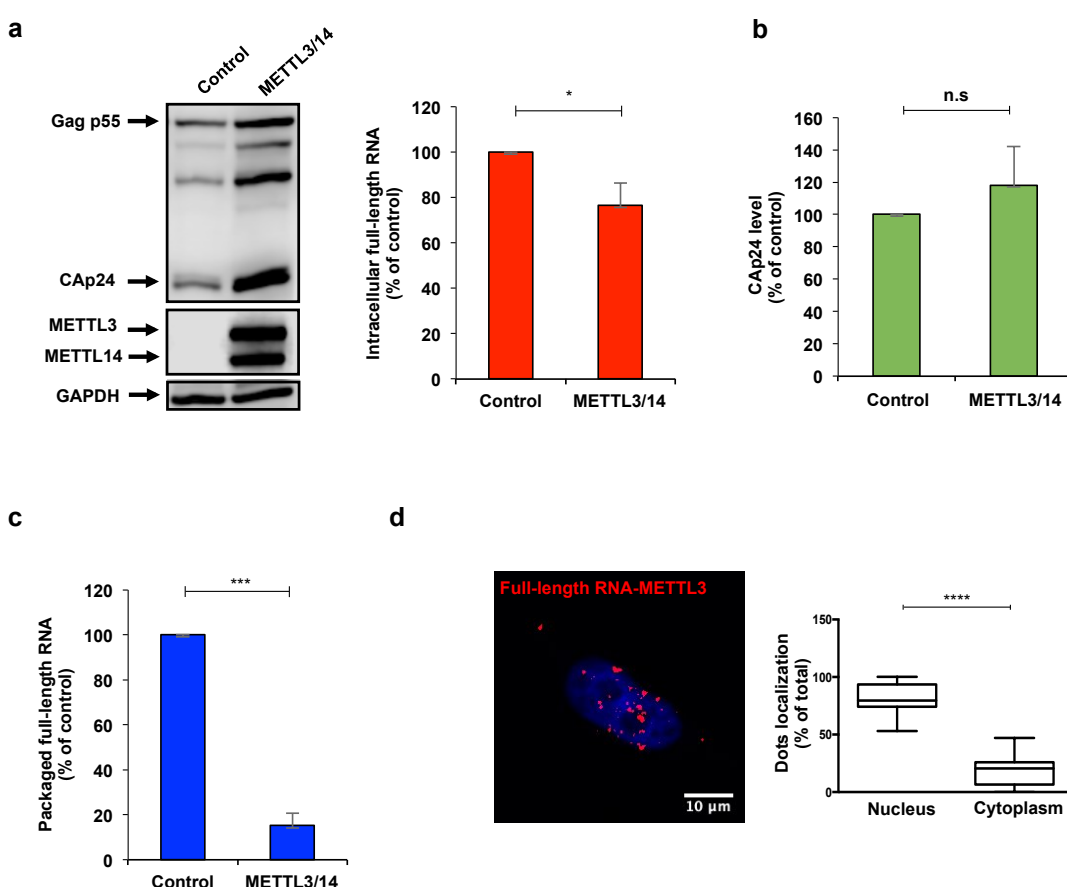
169 Together, these data indicate that the presence of m<sup>6</sup>A may play an important role in the  
170 folding and dimerization of the 5'-UTR and prompted us to study this feature in a cellular  
171 context.

172

### 173 **The presence of m<sup>6</sup>A within the full-length RNA favors Gag synthesis but interferes with 174 packaging**

175 In order to study the role of m<sup>6</sup>A on the cytoplasmic fate of the full-length RNA during viral  
176 replication, we first determined the effects of METTL3/14 overexpression on Gag and full-  
177 length RNA levels obtained from cell extracts and purified viral particles (see scheme in  
178 Supplementary Fig. 2a). m<sup>6</sup>A-RIP analysis from METTL3/14 overexpressing cells showed an  
179 increase in the m<sup>6</sup>A/A ratio of the full-length RNA compared to the control indicating that the  
180 viral transcript is hypermethylated under these experimental conditions (Supplementary Fig.  
181 2b). Consistent with the positive role of m<sup>6</sup>A on Gag synthesis previously described<sup>20-22</sup>, we  
182 observed that increased methylation of the full-length RNA by METTL3/14 overexpression  
183 results in increased levels of Gag and its processing products with minor effects on the

184 intracellular levels of the full-length RNA (Fig. 2a). Quantification of viral particles produced  
185 from the same cells revealed a slight increase in Gag levels (as judged by anti-CAp24 ELISA)  
186 from METTL3/14 overexpressing cells, which could be attributed to the increased Gag  
187 synthesis observed (Fig. 2b).



188  
189 **Figure 2: The presence of m<sup>6</sup>A within the full-length RNA favors Gag synthesis but interferes with packaging.**  
190 HEK293T cells were transfected with pNL4.3 and pCMV-VSVg together with pCDNA-Flag-METTL3 and pCDNA-Flag-  
191 METTL14 or pCDNA-d2EGFP as a control. **a**, At 24 hpt cells extracts were used to detect Gag, Flag-METTL3 and Flag-  
192 METTL14 by Western blot. GAPDH was used as a loading control (left panel). In parallel, cells extracts were used to  
193 perform RNA extraction and the full-length RNA was quantified by RT-qPCR (right panel). Intracellular full-length RNA  
194 was normalized to the control (arbitrary set to 100%) and presented as the mean +/- SD of three independent experiments  
195 (\*P<0.05, t-test). **b**, Supernatants from cell cultures in (a) were filtered and viral particles were purified by  
196 ultracentrifugation. The level of CAp24 was quantified by an anti-CAp24 ELISA. The level of CAp24 was normalized to the  
197 control (arbitrary set to 100%) and presented as the mean +/- SD of three independent experiments (n.s; non-significant, t-  
198 test). **c**, Viral particles purified from (b) were used to perform RNA extraction and the packaged full-length RNA from  
199 CAp24 equivalents was quantified by RT-qPCR. Packaged full-length RNA was normalized to the control (arbitrary set to  
200 100%) and presented as the mean +/- SD of three independent experiments (\*\*P<0.001, t-test). **d**, HeLa cells were  
201 transfected with pNL4.3, pCMV-VSVg and pCDNA-Flag-METTL3. At 24 hpt, the interaction between the full-length RNA  
202 and the Flag-tagged METTL3 was analyzed by ISH-PLA as described in the Methods section. Red dots indicate the  
203 interactions between the full-length RNA and the METTL3. Scale bar 10 mm. A quantification of the red dots in the nucleus

204 (co-localizing with the DAPI staining) and the cytoplasm of 14 cells is presented on the right (\*\*\*\* $P<0.0001$ , Mann-  
205 Whitney test).

206  
207 Then, we quantified the full-length RNA from equal amounts of viral particles and observed  
208 that viral particles produced under METTL3/14 overexpression contain around 3-fold less  
209 packaged gRNA indicating that hypermethylation of the full-length RNA impedes its  
210 packaging into nascent particles (Fig. 2c). We were not able to observe a similar effect of  
211 murine METTL3/14 overexpression on the simple retrovirus MLV, which was shown two  
212 segregate their full-length RNA into two specialized populations for translation and  
213 packaging further suggesting that MLV and HIV-1 might evolved diverse mechanisms for the  
214 cytoplasmic sorting of their full-length RNA (Supplementary Fig. 2c).

215 Since results presented above indicate that m<sup>6</sup>A deposition by METTL3/14 affects the  
216 cytoplasmic fate of the full-length RNA, we wanted to investigate where within the cell the  
217 m<sup>6</sup>A writer complex modifies the viral RNA. For this, we analyzed the interaction between  
218 the full-length RNA and METTL3 by *in situ* hybridization coupled to the proximity ligation  
219 assay (ISH-PLA)<sup>24</sup>. Confocal microscopy analyses revealed a predominant interaction within  
220 the nucleus, which suggests that the full-length RNA must be methylated in the nucleus and  
221 reach the cytoplasm in a methylated form (Fig. 2d and Supplementary Fig. 2d).

222 Together, these data suggest that nuclear methylation of the HIV-1 full-length RNA by  
223 METTL3/14 favors its use as mRNA for Gag synthesis but interferes with its incorporation  
224 into viral particles.

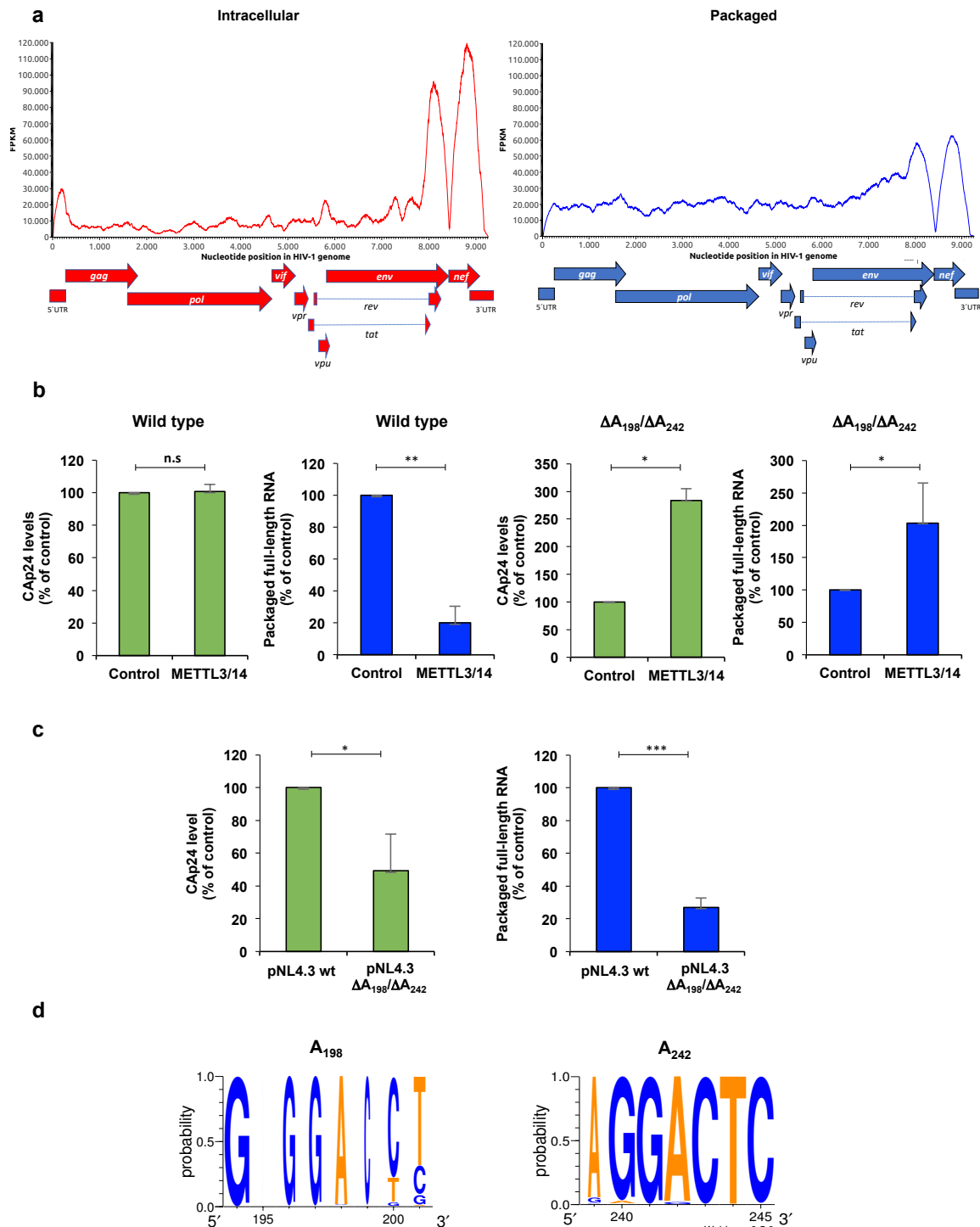
225  
226 **Methylation of A<sub>198</sub> and A<sub>242</sub> within the 5'-UTR interferes with HIV-1 full-length RNA  
227 packaging**

228 From data presented above, it seems that the presence of m<sup>6</sup>A interferes with the function of  
229 the HIV-1 full-length RNA as gRNA. Thus, to gain further insights into this regulation, we  
230 employed the m<sup>6</sup>A-seq strategy to determine the m<sup>6</sup>A patterns of the intracellular and viral  
231 particle-associated HIV-1 full-length RNA. In agreement with previous data reported for the  
232 NL4.3 and LAI.2 strains in T-lymphocytes and HEK293T cells<sup>20-22</sup>, we identified m<sup>6</sup>A peaks  
233 mainly at the 5'-UTR and a cluster of peaks at the 3' end of the intracellular full-length RNA  
234 (Fig. 3a, see intracellular full-length RNA). Interestingly, we observed that the full-length  
235 RNA from purified viral particles maintains the m<sup>6</sup>A peak at the 3'-UTR but lacks the m<sup>6</sup>A  
236 peak at the 5'-UTR. This observation together with data from Fig. 2c suggests that the  
237 presence of m<sup>6</sup>A at the 5'-UTR interferes with the incorporation of the full-length RNA into

238 viral particles (Fig. 3a, see packaged full-length RNA). Of note, this difference in the  
239 methylation patterns between intracellular and packaged RNA was not observed in the host  
240 7SL RNA, which is also packaged at high levels into HIV-1 particles <sup>25</sup>, indicating a very  
241 specific effect of m<sup>6</sup>A on full-length RNA packaging (Supplementary Fig. 3a). These data  
242 strongly suggest that full-length RNA molecules lacking m<sup>6</sup>A at the 5'-UTR are primarily  
243 selected by Gag as gRNA to be incorporated into viral particles.

244 A bioinformatic prediction of the potentially methylated residues within the 5'-UTR of the  
245 NL4.3 strain identified A<sub>198</sub> and A<sub>242</sub> in a very favorable methylation context (Supplementary  
246 Fig. 3b). Both residues are contained within the m<sup>6</sup>A peak we have identified within the 5'-  
247 UTR of the intracellular full-length RNA (Supplementary Fig. 3c) and were also identified in  
248 previous m<sup>6</sup>A-seq data obtained from T-lymphocytes and HEK293T cells <sup>20, 22</sup>. Thus, we  
249 deleted A<sub>198</sub>, A<sub>242</sub> or both from the NL4.3 provirus in order to determine the role of these  
250 adenosine residues on the m<sup>6</sup>A-mediated regulation of full-length RNA packaging. We  
251 observed that ΔA<sub>198</sub> and ΔA<sub>242</sub> single mutant proviruses were slightly resistant to the effects  
252 of METTL3/14 overexpression on full-length RNA packaging (Supplementary Fig. 3d).  
253 However, the ΔA<sub>198</sub>/ΔA<sub>242</sub> double mutant provirus was refractory to the positive effects of  
254 METTL3/14 overexpression on Gag synthesis and the negative effects on full-length RNA  
255 packaging observed with the wild type provirus indicating that A<sub>198</sub> and A<sub>242</sub> are key residues  
256 involved in this m<sup>6</sup>A-mediated regulation (Fig. 3b and Supplementary Fig. 3e). Next, we  
257 sought to investigate the role of A<sub>198</sub> and A<sub>242</sub> on HIV-1 full-length RNA metabolism. A  
258 comparison between wild type and the ΔA<sub>198</sub>/A<sub>242</sub> provirus showed that the double mutant  
259 virus accumulates more intracellular Gag but releases significantly less viral particles (Fig. 3c  
260 and Supplementary Fig. 3f). Moreover, quantification of the full-length RNA from equal  
261 amounts of viral particles revealed a defect in packaging in the ΔA<sub>198</sub>/A<sub>242</sub> double mutant  
262 provirus thus, confirming the critical relevance of these two adenosine residues for the  
263 incorporation of the HIV-1 full-length RNA into viral particles (Fig. 3c). An analysis of 890  
264 sequences from the HIV database ([www.hiv.lanl.gov](http://www.hiv.lanl.gov)) indicate that A<sub>198</sub> and A<sub>242</sub> are highly  
265 conserved within the 5'-UTR of isolates suggesting that this epitranscriptomic regulation  
266 must be a common feature of different HIV-1 subtypes including the highly prevalent  
267 subtypes C and B as well as circulating recombinant forms (Fig. 3d and Supplementary Fig.  
268 3g). Taking together, these results indicate that the HIV-1 full-length RNA may exist as two  
269 different populations that differ at least in the m<sup>6</sup>A residues present within the 5'-UTR. Only

270 the full-length RNA molecules lacking  $\text{m}^6\text{A}$  at positions 198 and 242 might be recognized by  
 271 Gag for packaging.



272  
 273 **Figure 3: Methylation of  $\text{A}_{198}$  and  $\text{A}_{242}$  within the 5'-UTR interferes with HIV-1 full-length RNA packaging.** a,  
 274 HEK293T cells were transfected with pNL4.3 and pCMV-VSVg. Intracellular polyA RNA or viral particle-associated RNA  
 275 was extracted at 24 hpt, fragmented and used for  $\text{m}^6\text{A}$ -seq as described in Methods. Peak calling results for the intracellular  
 276 (left) and packaged (right) full-length RNA is shown. b, HEK293T cells were transfected with pNL4.3 wild type or pNL4.3

277 DA<sub>198</sub>/DA<sub>242</sub> together with pCMV-VSVg, pCDNA-Flag-METTL3 and pCDNA-Flag-METTL14 or pCDNA-d2EGFP as a  
278 control. At 24 hpt supernatants were filtered and viral particles were purified by ultracentrifugation. Purified viral particles  
279 were used to perform an anti-CAp24 ELISA and RNA extraction and RT-qPCR analysis as described above. The levels of  
280 CAp24 and the packaged full-length RNA (per CAp24 equivalents) were normalized to the control (arbitrary set to 100%)  
281 and presented as the mean +/- SD of three independent experiments (\*P<0.05; \*\*P<0.01; n.s, non-significant, *t*-test). **c**,  
282 HEK293T cells were transfected with pNL4.3 wild type or pNL4.3 DA<sub>198</sub>/DA<sub>242</sub> together with pCMV-VSVg and the  
283 supernatant was filtered and ultracentrifuged at 24 hpt. Purified viral particles were used to perform an anti-CAp24 ELISA  
284 and for RNA extraction and RT-qPCR analysis as described above. The levels of CAp24 and the packaged full-length RNA  
285 (per CAp24 equivalents) were normalized to the control (arbitrary set to 100%) and presented as the mean +/- SD of three  
286 independent experiments (\*P<0.05; \*\*\*P<0.001, *t*-test). **d**, Conservation analyses of adenosines 198 and 242 from 879  
287 sequences from the HIV-1 database.

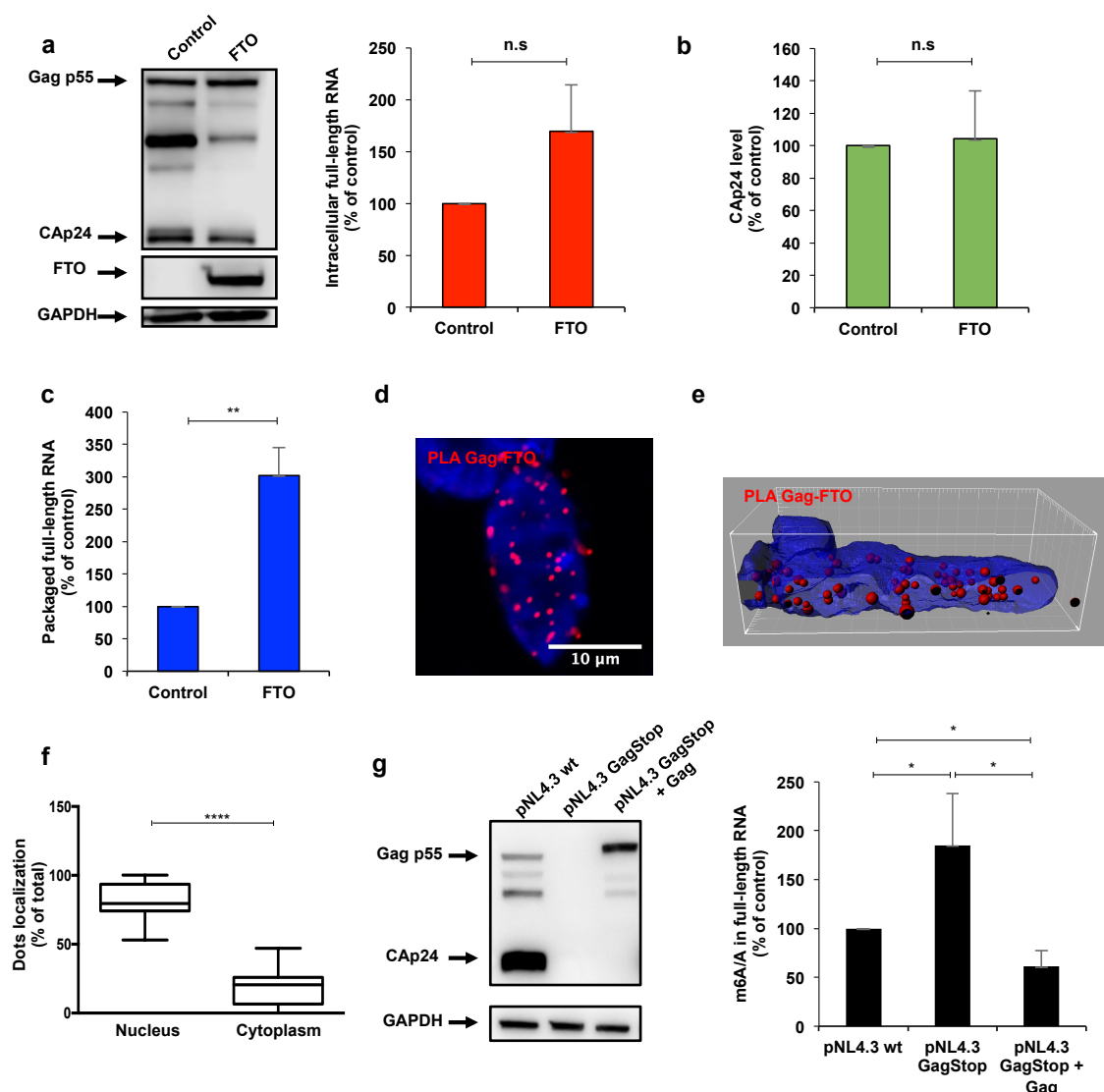
288

## 289 **Demethylation by a Gag-FTO complex favors HIV-1 full-length RNA packaging**

290 Then, we sought to determine whether this m<sup>6</sup>A-mediated regulation of full-length RNA  
291 packaging was a dynamic process. This was important considering that the reversible nature  
292 of adenosine methylation in cellular mRNA has been challenged <sup>26</sup>. For this, we  
293 overexpressed the RNA demethylase FTO and the analysis of the m<sup>6</sup>A/A ratio of the full-  
294 length RNA in control and FTO overexpressing cells revealed that the viral RNA is indeed a  
295 substrate for this m<sup>6</sup>A eraser (Supplementary Fig. 4a). Consistent with a positive role of m<sup>6</sup>A  
296 on Gag synthesis, we observed that FTO-induced demethylation of the full-length RNA  
297 results in a reduction of Gag levels despite a slight increase in intracellular full-length RNA  
298 levels (Fig. 4a). We also observed minimal changes in the CAp24 levels from purified viral  
299 particles produced under RNA demethylation conditions (Fig. 4b). However and in agreement  
300 with a negative role of m<sup>6</sup>A on full-length RNA packaging, we observed that viral particles  
301 produced from FTO overexpressing cells contain around 3-fold more packaged gRNA  
302 compared to the control (Fig. 4c). It should be mentioned that we were not able to observe  
303 similar results with the RNA demethylase ALKBH5 suggesting that full-length RNA  
304 demethylation by FTO is important for packaging (Supplementary Fig. 4b).

305 Considering that m<sup>6</sup>A demethylation favors full-length RNA packaging, we wanted to know  
306 where within the cell the viral RNA became demethylated by FTO. For this, we analyzed the  
307 interaction of the between the full-length RNA and FTO in cells by ISH-PLA but despite  
308 several attempts, we were not able to detect a direct interaction regardless all the components  
309 were correctly expressed within the cells (Supplementary Fig. 4c). This observation suggests  
310 that either there is no a massive interaction between the full-length RNA and FTO or that such  
311 interactions occurs very transiently (or at very low rates) being below the detection limit of  
312 our ISH-PLA strategy.

313 The lack of a detectable interaction between the full-length RNA and FTO prompted us to  
 314 investigate whether Gag could interact with FTO and drive full-length RNA demethylation. In  
 315 order to test this possibility, we employed the proximity ligation assay (PLA) and observed  
 316 that Gag and FTO indeed form complexes in cells (Fig. 4d). Interestingly, quantification of  
 317 the dots per cell localizing with the nuclear staining as well as 3D reconstitutions of  
 318 representative images indicate that Gag and FTO mostly associates within the nucleus (Figs.  
 319 4e and 4f). Indeed, we observed that FTO overexpression increases the nuclear localization  
 320 of Gag (Supplementary Fig. 4d).



321 **Figure 4: Demethylation by a Gag-FTO complex favors HIV-1 full-length RNA packaging.** HEK293T cells were  
 322 transfected with pNL4.3 and pCMV-VSVg together with pCDNA-3XFlag-FTO or pCDNA-3XFlag-d2EGFP as a control. **a**,  
 323 At 24 hpt cells extracts were used to detect Gag and 3XFlag-FTO by Western blot. GAPDH was used as a loading control  
 324 (left panel). In parallel, cells extracts were used to perform RNA extraction and the full-length RNA was quantified by RT-  
 325 qPCR (right panel). Intracellular full-length RNA was normalized to the control (arbitrary set to 100%) and presented as the  
 326 quantification of the dots per cell localizing with the nuclear staining as well as 3D reconstitutions of representative images  
 indicate that Gag and FTO mostly associates within the nucleus (Figs. 4e and 4f). Indeed, we observed that FTO  
 overexpression increases the nuclear localization of Gag (Supplementary Fig. 4d).

327 mean +/- SD of three independent experiments (\* $P<0.05$ , *t*-test). **b**, Supernatants from cell cultures in (a) were filtered and  
328 viral particles were purified by ultracentrifugation. The level of CAp24 was quantified by an anti-CAp24 ELISA, normalized  
329 to the control (arbitrary set to 100%) and presented as the mean +/- SD of three independent experiments (n.s; non-  
330 significant, *t*-test). **c**, Viral particles purified from (b) were used to perform RNA extraction and the packaged full-length  
331 RNA from CAp24 equivalents was quantified by RT-qPCR. Packaged full-length RNA was normalized to the control  
332 (arbitrary set to 100%) and presented as the mean +/- SD of three independent experiments (\*\* $P<0.01$ , *t*-test). **d**, HeLa cells  
333 were co-transfected with pNL4.3, pCMV-VSVg and pCDNA-3XFlag-FTO. At 24 hpt, the interaction between Gag and Flag-  
334 tagged FTO was analyzed by PLA as described in Methods. Red dots indicate the interactions between Gag and FTO (left  
335 panel). Scale bar 10 mm. **e**, Three-dimensional reconstitution of the PLA results shown in (d) was performed to determine the  
336 subcellular localization of the interaction between Gag and FTO. **f**, Quantification of the red dots in the nucleus (co-  
337 localizing with the DAPI staining) and the cytoplasm of 15 cells is presented on the right (\*\*\*\* $P<0,0001$ , Mann-Whitney  
338 test). **g**, HEK293T cells were transfected with the pNL4.3 wild type, pNL4.3-GagStop or pNL4.3-GagStop together with  
339 pCDNA-Gag. At 24 hpt cells extracts were used to detect Gag and GAPDH was used as a loading control. In parallel, cells  
340 extracts were used to perform RNA extraction followed by an immunoprecipitation using an anti-m<sup>6</sup>A antibody (m<sup>6</sup>A-RIP as  
341 described in Methods). The full-length RNA from the input ("A" fraction) and from the immunoprecipitated material ("m<sup>6</sup>A"  
342 fraction) was quantified by RT-qPCR. The m<sup>6</sup>A/A ratio was normalized to pNL4.3 wild type (arbitrary set to 100%) and  
343 presented as the mean +/- SD of three independent experiments (\* $P<0.05$ , *t*-test).

344

345 From these results, it was tempting to speculate that the full-length RNA is methylated within  
346 the nucleus by METLL3/14 and Gag interacts with FTO in the nucleus to drive demethylation  
347 of the full-length RNA molecules that will be incorporated into assembling viral particles.  
348 Thus, we analyzed the m<sup>6</sup>A content of the full-length RNA in the presence or absence of Gag  
349 by using the wild type NL4.3 provirus and a mutant provirus containing premature stops  
350 codons that abolish Gag synthesis (GagStop provirus). Compared to the wild type full-length  
351 RNA, the level of m<sup>6</sup>A increases when Gag is absent and is restored or even decreased when  
352 the Gag protein was expressed *in trans* indicating that Gag regulates the methylation status of  
353 the full-length RNA (Fig. 4g).

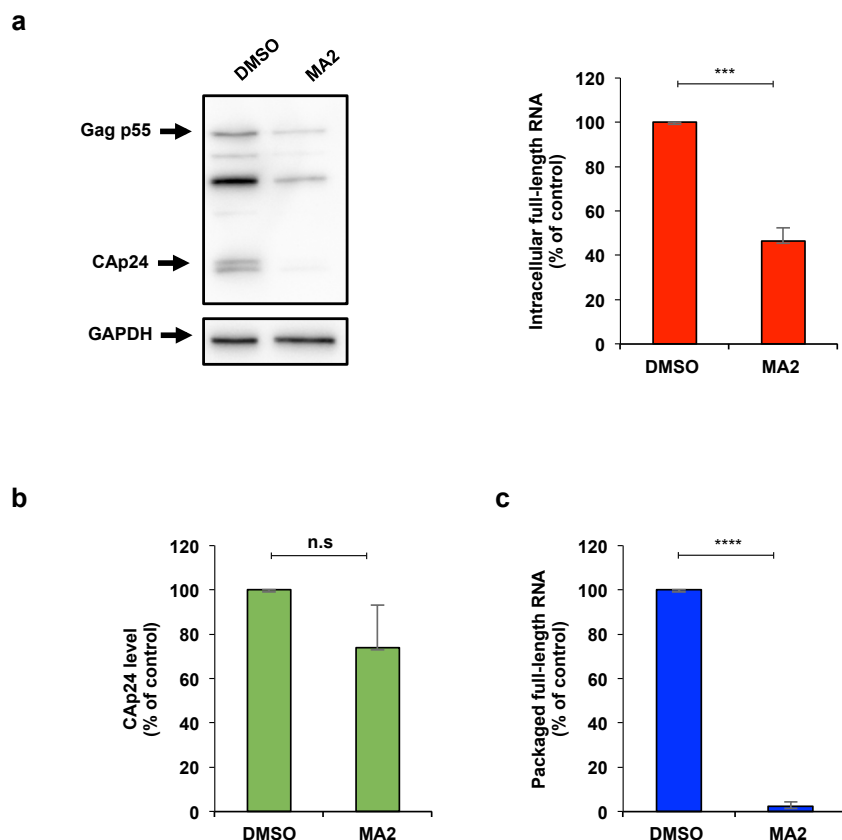
354 Together, these results strongly indicate that the FTO-mediated demethylation is required for  
355 full-length RNA packaging in a process supported by the Gag precursor.

356

### 357 **Inhibition of FTO demethylase activity impacts full-length RNA metabolism and blocks** 358 **packaging**

359 We finally sought to determine whether this epitranscriptomic regulation of the HIV-1 full-  
360 length RNA packaging was a potential therapeutic target for pharmacological intervention.  
361 For this, we took advantage of the ester form of meclofenamic acid (MA2), which was shown  
362 to specifically interfere with FTO-mediated m<sup>6</sup>A demethylation <sup>27</sup>. Therefore, we analyzed  
363 Gag and the full-length RNA in cells treated with DMSO (as a control) or MA2 and observed  
364 a reduction in Gag synthesis and the intracellular levels of the full-length RNA indicating that

365 FTO-mediated demethylation is required for proper metabolism of the full-length RNA within  
 366 the cell (Fig. 5a). Consistent with a perturbed intracellular full-length RNA metabolism, we  
 367 observed a decrease in the viral particles released from MA2-treated cells (Fig. 5b).  
 368 Strikingly, quantification of the packaged full-length RNA from equal amounts of viral  
 369 particles indicates that inhibition of FTO activity by MA2 almost abolished packaging (Fig.  
 370 5c).



371  
 372 **Figure 5: Inhibition of FTO demethylase activity impacts full-length RNA metabolism and blocks packaging.**  
 373 HEK293T cells were transfected with pNL4.3 and pCMV-VSVg and were treated with MA2 or DMSO as a control. **a**, At 24  
 374 hpt cells extracts were used to detect Gag and GAPDH as a loading control (left panel). In parallel, cells extracts were used to  
 375 perform RNA extraction and the full-length RNA was quantified by RT-qPCR (right panel). The intracellular full-length  
 376 RNA was normalized to the control (arbitrary set to 100%) and presented as the mean +/- SD of three independent  
 377 experiments (\*\*P<0.001, *t*-test). **b**, At 24 hpt the supernatant was filtered and viral particles were purified by  
 378 ultracentrifugation. The level of CAp24 was quantified by an anti-CAp24 ELISA, normalized to the control (arbitrary set to  
 379 100%) and presented as the mean +/- SD of three independent experiments (n.s; non-significant, *t*-test). **c**, Purified viral  
 380 particles from (b) were used to perform an RNA extraction and the packaged full-length RNA from CAp24 equivalents was  
 381 quantified by RT-qPCR. Packaged full-length RNA was normalized to the control (arbitrary set to 100%) and presented as  
 382 the mean +/- SD of three independent experiments (\*\*\*\*P<0.0001, *t*-test).

383

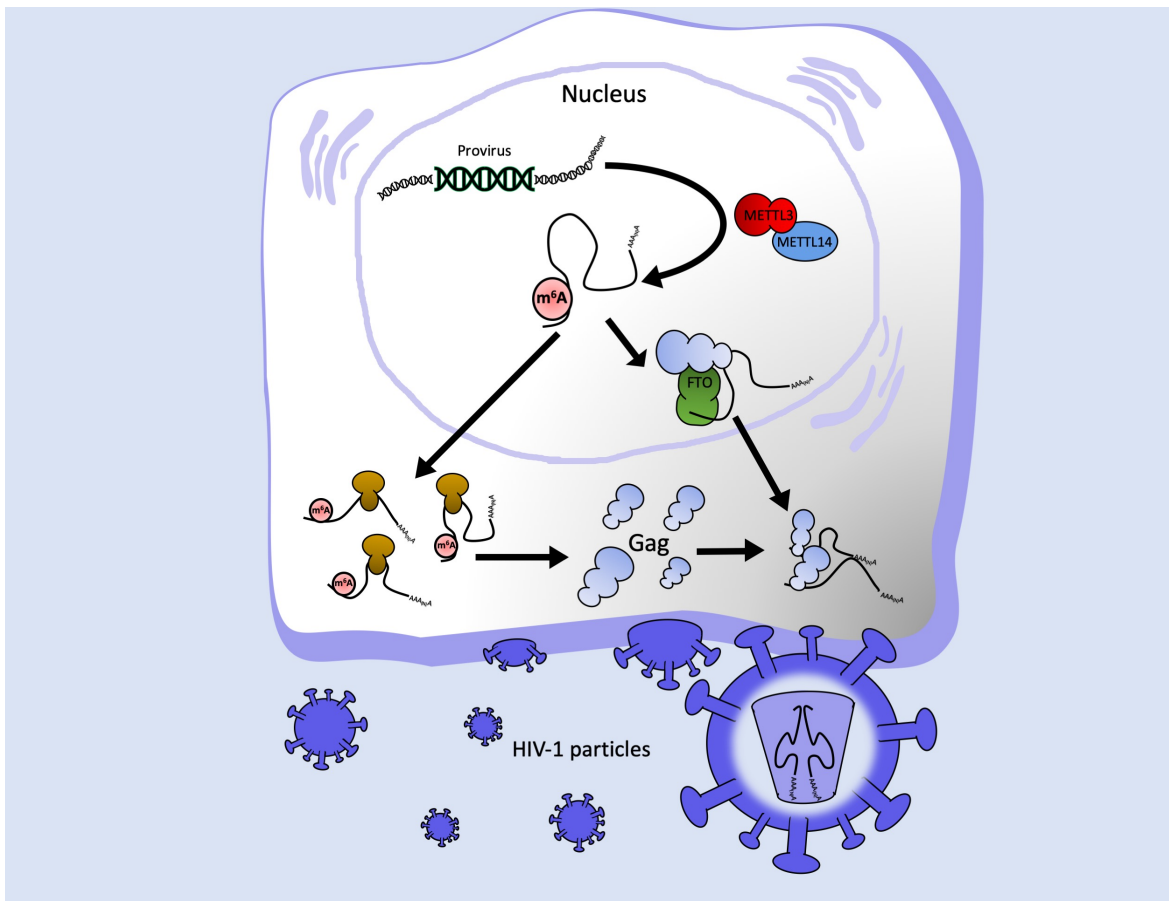
384 Taking together, these results confirm that FTO-mediated demethylation is critical for HIV-1  
385 full-length RNA packaging and this process is a potential target for the design of novel  
386 antiretroviral drugs.

387

## 388 **DISCUSSION**

389 Assembly of human immunodeficiency virus type-1 particles is a highly regulated process in  
390 which the major structural polyprotein Gag together with other viral and cellular components  
391 are recruited to the plasma membrane for the release of the viral progeny. The assembly  
392 process occurs in multiple steps driven by the different functional domains that compose the  
393 Gag precursor. As such, while the nucleoprotein (NC) domain specifically recruits two copies  
394 of the full-length RNA, the matrix (MA) domain allows targeting of the complex to specific  
395 plasma membrane micro-domains and the capsid (CA) domain drives Gag multimerization at  
396 such sites. Packaging of two copies of full-length RNA by the NC domain of Gag is highly  
397 specific and occurs selectively over thousands of cellular and viral RNA species. This  
398 selectivity was proposed to be possible by the presence of *cis*-acting RNA signatures  
399 spanning the 5'-UTR and the beginning of the Gag coding region. However, the full-length  
400 RNA also serves as mRNA for the synthesis of Gag and Gag-Pol precursors and thus,  
401 translation and packaging are expected to be two mutually exclusive processes. Although the  
402 adoption of a branched multiple hairpin (BMH) conformation of the 5'-UTR was initially  
403 proposed to favor dimerization and packaging over translation<sup>12-14</sup>, it was later demonstrated  
404 that translation of the full-length RNA is under positive selection and thus, not regulated by a  
405 conformational switch of the 5'-UTR<sup>18, 19</sup>. Additional structural studies carried out in cells  
406 and virions also argued against structural rearrangements as drivers of the transition between  
407 translation and packaging of the HIV-1 full-length RNA<sup>16, 17, 28</sup>. Therefore, the mechanism by  
408 which Gag selects “packageable” from “translatable” full-length RNA molecules still remains  
409 as one of the long-lasting questions in Retrovirology. In this work, we showed that  
410 demethylation of two highly conserved adenosine residues within the 5'-UTR is critical for  
411 packaging of the HIV-1 full-length RNA. Interestingly, we observed that Gag associates with  
412 the RNA demethylase FTO in the nucleus and promotes demethylation of the full-length  
413 RNA, suggesting that Gag may drive FTO-mediated demethylation of those RNA molecules  
414 that will be used as gRNA to be incorporated into assembling viral particles (Fig. 6). This  
415 differential epitranscriptomic regulation exerted on the full-length RNA depending on its  
416 functions (mRNA or gRNA) may also help to explain the controversies reported in the  
417 literature<sup>29</sup>. As such, while the presence of m<sup>6</sup>A favors Gag synthesis through YTHDF

418 proteins acting on the full-length RNA molecules destined to serve as mRNA<sup>21</sup>, the same  
419 cytoplasmic m<sup>6</sup>A readers may recognize specific features and drive degradation of the  
420 incoming viral RNA early upon infection (i.e., when the full-length RNA acts as gRNA)<sup>22</sup>.



421  
422 **Figure 6 Working model for the epitranscriptomic regulation of HIV-1 full-length RNA packaging.** The HIV-1 full-  
423 length RNA is methylated by METTL3/14 complex in the nucleus (for simplicity, only the presence of m<sup>6</sup>A on the 5'-UTR is  
424 shown). However, the structural protein Gag interacts with the m<sup>6</sup>A eraser FTO and drives demethylation of adenosines  
425 residues present at the 5'-UTR in a process required for full-length RNA packaging.

426  
427 Further studies are required to elucidate the mechanism by which the binding of YTHDF  
428 proteins to m<sup>6</sup>A residues negatively impact full-length RNA metabolism in the absence of  
429 translation and whether methylation of the 5'-UTR is involved. In addition, the molecular  
430 mechanism by which the presence of m<sup>6</sup>A at the 5'-UTR interferes with full-length RNA  
431 packaging also deserves further investigation. One of the most plausible explanations is that  
432 recognition of m<sup>6</sup>A residues at the 5'-UTR by reader proteins interferes with Gag binding  
433 and/or full-length RNA dimerization. However, it is also possible that the presence of m<sup>6</sup>A  
434 itself directly repeals the recruitment of Gag or alters the optimal RNA conformation of the  
435 dimerization and/or packaging signal. Indeed, our *in vitro* structural and dimerization analyses

436 support this last idea as they suggest that the presence of m<sup>6</sup>A affects the folding and  
437 dimerization of the 5'-UTR. Of note, although neither A<sub>198</sub> nor A<sub>242</sub> showed a significant  
438 reactivity alteration this does not exclude that their modification may have influenced the  
439 reactivity of close nucleotides such as G<sub>240</sub> and G<sub>241</sub>. To date no studies have monitored the  
440 effect of m<sup>6</sup>A on such a complex structure and here we clearly show that this modification can  
441 have not only local but more global effects on RNA folding. Indeed, we observed that the  
442 introduction of m<sup>6</sup>A alters dimerization of the 5'-UTR, which could at least partly explain  
443 why methylated full-length RNA are not recovered within viral particles. Nevertheless, our  
444 experiments using the  $\Delta A_{198}/\Delta A_{242}$  provirus strongly indicate that these two adenosine  
445 residues play a major role in packaging. While A<sub>198</sub> is located within the region  
446 complementary to the tRNA<sup>Lys3</sup> at the primer binding site (PBS), A<sub>242</sub> is located in the AGGA  
447 bulge at the base of the SL1 region and corresponds to a Gag-binding domain previously  
448 shown by chemical probing *in vitro* and *in virio* as well as by CLIP-seq studies<sup>17, 30, 31</sup>.  
449 Further studies are required to fully understand the role of these residues in full-length RNA  
450 packaging.

451 In contrast to the simple retrovirus MLV, which segregates its full-length RNA into two  
452 separate populations for translation and packaging, the full-length RNA of the human  
453 lentivirus HIV-1 was proposed to exist as a single population that can indistinctly serve as  
454 mRNA or gRNA. While the presence of two specialized full-length RNA populations  
455 supports the lack of an epitranscriptomic regulation of MLV packaging, our data obtained  
456 with HIV-1 suggest that its full-length RNA may also exist as two populations with different  
457 m<sup>6</sup>A patterns. From these two populations, those molecules lacking m<sup>6</sup>A at the 5'-UTR will  
458 be preferentially selected by Gag for packaging (Fig. 6). In this regard, the HCV core protein  
459 was also shown to bind preferentially to RNA molecules lacking m<sup>6</sup>A most probably to avoid  
460 YTHDF proteins-mediated degradation upon viral entry<sup>32</sup>. Whether the packaging of  
461 hypomethylated RNA genomes is a conserved mechanism evolved by RNA viruses to avoid  
462 early degradation by cytoplasmic m<sup>6</sup>A readers must be determined.

463 Although the reversibility of adenosine methylation as well as the main target of the RNA  
464 demethylase FTO have been recently challenged<sup>26, 33</sup>, we showed that the HIV-1 full-length  
465 RNA is a substrate for FTO and this RNA demethylase regulates the incorporation of the viral  
466 genome into released viral particles. Interestingly, treatment of HIV-1 producer cells with the  
467 specific FTO inhibitor meclofenamic acid resulted in an impairment of full-length RNA  
468 metabolism with a potent effect on packaging, confirming the critical role of the demethylase  
469 activity of FTO during viral replication. In addition to meclofenamic acid, two small

470 molecules developed by structure-based rational design were recently described as specific  
471 inhibitors of FTO m<sup>6</sup>A demethylase activity with the potential to be used as a treatment for  
472 adult myeloid leukemia <sup>34</sup>. Therefore, this novel epitranscriptomic mechanism regulating  
473 packaging of the HIV-1 full-length RNA could also be exploited as a target for  
474 pharmacological intervention.

475

## 476 METHODS

477 **Selective 2'-hydroxyl acylation analyzed by primer extension (SHAPE):** The HIV-1 full-  
478 length RNA 5'-UTR was *in vitro* transcribed using the T7 RNA polymerase as described <sup>35</sup>.  
479 For m<sup>6</sup>A RNAs, ATP was substituted by N<sup>6</sup>-methyl-ATP (Jena Bioscience). RNA was  
480 quantified by measurement of the OD<sub>256</sub> using a BioSpec-nano (Shimadzu). RNA integrity  
481 was assessed by agarose gel electrophoresis. SHAPE probing was conducted essentially as in  
482 <sup>17</sup> with minor modifications. Briefly, 6 pmol of *in vitro* transcribed RNA containing 100%  
483 m<sup>6</sup>A or 0% m<sup>6</sup>A were diluted in 24  $\mu$ l of water, denatured at 80°C for 2 minutes and ice  
484 cooled. After addition of 3  $\mu$ l of 10X Folding Buffer (HEPES Ph7.5 400 nM, KCl 1M, MgCl<sub>2</sub>  
485 50 mM), samples were incubated for 10 minutes at room temperature and then 10 minutes at  
486 37°C. Then, the RNA solution was added to 3  $\mu$ l of 20 mM 1M7 (2mM final) (AEchem  
487 Scientific Corporation) or to 3  $\mu$ l of DMSO (control) and incubated for 6 minutes at 37°C.  
488 RNA was subsequently precipitated in presence of 1  $\mu$ l of 20 mg/ml of glycogen, 3  $\mu$ l of 5M  
489 sodium acetate, 100  $\mu$ l of ETOH for 1 hour at -20°C and then washed with ETOH 70% and  
490 resuspended in water. For primer extension, RNA was treated with 1  $\mu$ l of DMSO and  
491 denatured for 3 minutes at 95°C and cooled at 4°C. Samples were mixed with 3  $\mu$ l of 2 $\mu$ M  
492 fluorescent primer (D4-5'-TTTCTTCCCCCTGGCCTT for the probed/control samples and  
493 D2-5'-TTTCTTCCCCCTGGCCTT for the sequencing reaction, Sigma) and incubated for 5  
494 minutes at 65°C, 10 minutes at 35°C and then 1 minute on ice. 5  $\mu$ l of Reverse Transcription  
495 Mix (10  $\mu$ l of 10 mM dNTPs and 40  $\mu$ l of 5X MMLV RT Buffer Promega), 1  $\mu$ l of 10 mM  
496 ddTTP for the sequencing reaction and 1  $\mu$ l of MMLV Reverse Transcriptase RNase H  
497 minus (Promega) were finally added and the reverse transcription was performed at 35°C for  
498 2 minutes, 42°C for 30 minutes and 55°C for 5 minutes. Samples were then ice cooled and  
499 precipitated with ETOH for 2 hours. Pellets were resuspended in 40  $\mu$ l of Sample Loading  
500 Solution (Beckman Coulter). Reverse transcription products were resolved on a CEQ-8000  
501 sequencer (Beckman Coulter). Electropherograms were analyzed using QuSHAPE <sup>36</sup>. Raw  
502 data were processed by excluding the 2% of the highest values and normalizing the remaining

503 values by the mean of the next 8% highest values <sup>37</sup>. The experiments were performed three  
504 times and reproducibility was assessed by calculating the standard error of the mean.  
505 Secondary structure was drawn using VaRNA <sup>38</sup>.

506

507 **Dimerization assay:** *In vitro* transcribed 5`-UTR was serially diluted in 10 mM Tris pH 7, 10  
508 mM NaCl, 140 mM KCl to obtain a final concentration ranging from 0 to 1  $\mu$ M. 20 fmol (2  
509 nM final) of radiolabeled RNA was added. Samples were denatured at 95°C for 3 minutes and  
510 then ice cooled. After addition of 1 mM MgCl<sub>2</sub>, RNA was allowed to fold for 30 minutes at  
511 37°C. Samples were subsequently chilled on ice, mixed with a 5X native loading buffer  
512 (glycerol 20%, xylene cyanol 0.1%, bromophenol blue 0.1%) and loaded on a native 4%  
513 acrylamide gel. Samples were run for 1 hour at 100V on 4% native acrylamide mini-gels  
514 containing 34 mM Tris, 54 mM HEPES, 0.1 mM EDTA and 2.5 mM MgCl<sub>2</sub>. Dried gels were  
515 quantified using a BAS-5000 phosphorimager and MultiGauge 3.0 (Fujifilm). The fraction of  
516 dimer was calculated as the ratio “dimer – background” over “dimer + monomer –  
517 2\*background”. Data were fitted to Fraction dimer = Bmax\*[RNA]/(Kd+[RNA]) using Prism  
518 5.02 (GraphPad Software).

519

520 **Cell culture, DNA transfection and viral particle purification:** HEK293T and HeLa cells  
521 were maintained in DMEM (Life technologies) supplemented with 10% FBS (Hyclone) and  
522 antibiotics (Hyclone) at 37°C and 5% CO<sub>2</sub> atmosphere. Cells growing in 6-well plates  
523 ( $2.5 \times 10^5$  cells/well) were transfected using linear PEI ~25000 Da (Polyscience) as described  
524 previously <sup>24</sup>. Cells were transfected using a ratio  $\mu$ g DNA/ $\mu$ l PEI of 1/15 and the DNA/PEI  
525 mix was incubated for 20 min at room temperature before adding to the cells. For experiments  
526 involving the FTO inhibitor, the culture medium was replaced by medium containing  
527 dimethyl sulfoxide (DMSO) as a control or 80  $\mu$ M of an ethyl ester form of meclofenamic  
528 acid diluted in DMSO (MA2) prior DNA transfection. For viral particle purification, the  
529 supernatant was collected and filtered by passing through a 0.22  $\mu$ m filter and then  
530 ultracentrifugated at 25.000 rpm for 2 hours at 4°C in a 20% sucrose cushion (prepared  
531 previously and stored at 4 °C). Purified viral particles were resuspended in 100  $\mu$ l of PBS and  
532 stored in aliquots at -80 °C to then perform anti-CAp24 ELISA (HIV-1) or Western blot  
533 (MLV) or RNA extraction. Cells were also collected to perform Western blot and RNA  
534 extraction as described in Supplementary Methods.

535

536 **m<sup>6</sup>A-seq:** Poly(A) RNA was purified from 100 µg of total RNA extracted from HEK293T  
537 cells previously transfected with pNL4.3 and pCMV-VSVg. Briefly, total RNA in 500 µl of  
538 water was incubated at 65°C for 10 minutes and incubated with 3 µl of oligo dT-Biotin (dT-B;  
539 IDT Technologies) (50 pmol/µl) and 13 µl of SSC Buffer 20X (Santa Cruz Biotechnology)  
540 and allowed to cool at room temperature. 600 µg of Dynabeads® Streptavidin (60 µl; Thermo  
541 Fisher) were washed three times with Buffer SSC 0.5X and resuspended in 100 µl of Buffer  
542 SSC 0.5X. Then, the RNA/oligo dT-B mix was incubated with the streptavidin beads at room  
543 temperature for 10 minutes in head-over-tail rotation. RNA-beads were washed four times  
544 with 300 µl Buffer SSC 0.1X and bound RNA was eluted twice with 100 µl of water. The  
545 RNA was precipitated with 10 mM MgCl<sub>2</sub>, 20 µg glycogen (Thermo Fisher) and 2.5 volume  
546 of ETOH 100% overnight at -20 °C and then washed with ETOH 70%. Poly(A) RNA as well  
547 as RNA obtained from purified viral particle were fragmented using Fragmentation Reagent  
548 (Thermo Fisher). For this, 2 µg of RNA in 9 µl of water was incubated with 1 µl of  
549 Fragmentation Buffer 10X for 15 minutes at 70 °C, then 1 µl of Stop solution was added and  
550 incubated on ice. The RNA fragmented was precipitated overnight as described above.  
551 Fragmented RNA diluted in 380 µl was heated at 70 °C for 5 minutes, placed on ice for 3  
552 minutes. The denatured RNA was mixed with 1 µl of rRNasin® (Promega), 5 µl VRC, 100 µl  
553 of IP Buffer 5X (50 mM Tris-HCl pH7.4, 750 mM NaCl and 0.5% NP-40) and 5 µl of an anti-  
554 m<sup>6</sup>A antibody (0,5 mg/mL; Synaptic System #202003) and incubated for 2 hours at 4 °C with  
555 head-over-tail rotation. At the same time, 600 µg of Dynabeads® Protein A magnetic beads  
556 (20 µl; Thermo Fisher) were washed in 1 ml of IP Buffer 1X with 1 µl of VRC and were  
557 incubated with 500 µl of Buffer IP 1X with 0.5 mg/ml of BSA for 2 hours at 4 °C with head-  
558 over-tail rotation. Then, beads were washed with 500 µl of IP Buffer 1X and added to the  
559 RNA/anti-m<sup>6</sup>A antibody mix. The RNA-beads mix was incubated for 2 hours at 4°C in head-  
560 over-tail rotation. After incubation, the RNA-beads mix was washed twice with 500 µl IP  
561 Buffer 1X. Bound RNA was eluted with 100 µl of Elution Buffer (5mM Tris-HCl, 1mM  
562 EDTA and 0.05% SDS) and 1 µl of Proteinase K (New England BioLabs) and incubated for  
563 1.5 hour at 50°C. RNA was extracted from supernatant using TRIzol® (ThermoFisher). The  
564 RNA recovered was precipitated with 10 mM MgCl<sub>2</sub>, 20 µg glycogen (Thermo Fisher) and  
565 2.5 volumes of ETOH 100% overnight at -20 °C and then washed with ETOH 70%. Equal  
566 amounts of RNA from input and immunoprecipitation were used for RT-qPCR. cDNA  
567 libraries preparations and RNAseq was performed at Genoma Mayor. All the samples were

568 sequenced in an Illumina HiSeq2000 platform with paired-end 100 bp read length. Read  
569 quality was evaluated with *Fastqc* and the *Burrows-Wheeler Alignment Tool (BWA -Mem)*  
570 was used for mapping reads to the HIV-1 genome with default parameters.  
571 The alignment data were analyzed with *MACS2* to call peaks with *-f BAMPE --nomodel --*  
572 *SPMR* options for generated viral peaks data and to generate FPKM (Fragments Per Kilobase  
573 per Million mapped reads). Predicted peaks were sorted by average coverage.

574

## 575 **DATA AVAILABILITY**

576 m<sup>6</sup>A-seq data were deposited at the GEO upon accession number GSE130687.  
577

## 578 **REFERENCES**

- 579 1. Karn, J. & Stoltzfus, C.M. Transcriptional and posttranscriptional regulation of  
580 HIV-1 gene expression. *Cold Spring Harbor Perspectives in Medicine* **2**, a006916  
581 (2012).
- 582 2. Butsch, M. & Boris-Lawrie, K. Destiny of unspliced retroviral RNA: ribosome  
583 and/or virion? *J Virol* **76**, 3089-3094 (2002).
- 584 3. Mailler, E. *et al.* The Life-Cycle of the HIV-1 Gag-RNA Complex. *Viruses* **8** (2016).
- 585 4. Levin, J.G., Grimley, P.M., Ramseur, J.M. & Berezesky, I.K. Deficiency of 60 to 70S  
586 RNA in murine leukemia virus particles assembled in cells treated with  
587 actinomycin D. *J Virol* **14**, 152-161 (1974).
- 588 5. Levin, J.G. & Rosenak, M.J. Synthesis of murine leukemia virus proteins associated  
589 with virions assembled in actinomycin D-treated cells: evidence for persistence  
590 of viral messenger RNA. *Proc Natl Acad Sci U S A* **73**, 1154-1158 (1976).
- 591 6. Dorman, N. & Lever, A. Comparison of viral genomic RNA sorting mechanisms in  
592 human immunodeficiency virus type 1 (HIV-1), HIV-2, and Moloney murine  
593 leukemia virus. *J Virol* **74**, 11413-11417. (2000).
- 594 7. Berkhout, B. Structure and function of the human immunodeficiency virus leader  
595 RNA. *Prog Nucleic Acid Res Mol Biol* **54**, 1-34 (1996).
- 596 8. Kuzembayeva, M., Dilley, K., Sardo, L. & Hu, W.S. Life of psi: how full-length HIV-1  
597 RNAs become packaged genomes in the viral particles. *Virology* **454-455**, 362-  
598 370 (2014).
- 599 9. Laughrea, M. *et al.* Mutations in the kissing-loop hairpin of human  
600 immunodeficiency virus type 1 reduce viral infectivity as well as genomic RNA  
601 packaging and dimerization. *J Virol* **71**, 3397-3406 (1997).
- 602 10. Chen, J. *et al.* HIV-1 RNA genome dimerizes on the plasma membrane in the  
603 presence of Gag protein. *Proc Natl Acad Sci U S A* **113**, E201-208 (2016).
- 604 11. Clever, J.L. & Parslow, T.G. Mutant human immunodeficiency virus type 1  
605 genomes with defects in RNA dimerization or encapsidation. *J Virol* **71**, 3407-  
606 3414 (1997).
- 607 12. Huthoff, H. & Berkhout, B. Two alternating structures of the HIV-1 leader RNA.  
608 *RNA* **7**, 143-157 (2001).
- 609 13. Berkhout, B. *et al.* In vitro evidence that the untranslated leader of the HIV-1  
610 genome is an RNA checkpoint that regulates multiple functions through  
611 conformational changes. *J Biol Chem* **277**, 19967-19975 (2002).

612 14. Abbink, T.E. & Berkhout, B. A novel long distance base-pairing interaction in  
613 human immunodeficiency virus type 1 RNA occludes the Gag start codon. *J Biol  
614 Chem* **278**, 11601-11611 (2003).

615 15. Keane, S.C. *et al.* RNA structure. Structure of the HIV-1 RNA packaging signal.  
616 *Science* **348**, 917-921 (2015).

617 16. Paillart, J.C. *et al.* First Snapshots of the HIV-1 RNA Structure in Infected Cells and  
618 in Virions. *J Biol Chem* **279**, 48397-48403 (2004).

619 17. Wilkinson, K.A. *et al.* High-throughput SHAPE analysis reveals structures in HIV-1  
620 genomic RNA strongly conserved across distinct biological states. *PLoS Biol* **6**,  
621 e96 (2008).

622 18. Abbink, T.E., Ooms, M., Haasnoot, P.C. & Berkhout, B. The HIV-1 leader RNA  
623 conformational switch regulates RNA dimerization but does not regulate mRNA  
624 translation. *Biochemistry* **44**, 9058-9066 (2005).

625 19. Boeras, I. *et al.* The basal translation rate of authentic HIV-1 RNA is regulated by  
626 5'UTR nt-pairings at junction of R and U5. *Sci Rep* **7**, 6902 (2017).

627 20. Lichinchi, G. *et al.* Dynamics of the human and viral m(6)A RNA methylomes  
628 during HIV-1 infection of T cells. *Nat Microbiol* **1**, 16011 (2016).

629 21. Kennedy, E.M. *et al.* Posttranscriptional m(6)A Editing of HIV-1 mRNAs Enhances  
630 Viral Gene Expression. *Cell Host Microbe* **19**, 675-685 (2016).

631 22. Tirumuru, N. *et al.* N(6)-methyladenosine of HIV-1 RNA regulates viral infection  
632 and HIV-1 Gag protein expression. *eLife* **5** (2016).

633 23. Lu, W. *et al.* N(6)-methyladenosine-binding proteins suppress HIV-1 infectivity  
634 and viral production. *J Biol Chem* (2018).

635 24. Toro-Ascuy, D. *et al.* A Rev-CBP80-eIF4AI complex drives Gag synthesis from the  
636 HIV-1 unspliced mRNA. *Nucleic Acids Res* **46**, 11539-11552 (2018).

637 25. Onafuwa-Nuga, A.A., Telesnitsky, A. & King, S.R. 7SL RNA, but not the 54-kd signal  
638 recognition particle protein, is an abundant component of both infectious HIV-1  
639 and minimal virus-like particles. *RNA* **12**, 542-546 (2006).

640 26. Darnell, R.B., Ke, S. & Darnell, J.E., Jr. pre-mRNA processing includes N6  
641 methylation of adenosine residues that are retained in mRNA exons and the  
642 fallacy of "RNA epigenetics". *RNA* (2017).

643 27. Huang, Y. *et al.* Meclofenamic acid selectively inhibits FTO demethylation of m6A  
644 over ALKBH5. *Nucleic Acids Res* **43**, 373-384 (2015).

645 28. Watts, J.M. *et al.* Architecture and secondary structure of an entire HIV-1 RNA  
646 genome. *Nature* **460**, 711-716 (2009).

647 29. Riquelme-Barrios, S., Pereira-Montecinos, C., Valiente-Echeverria, F. & Soto-Rifo,  
648 R. Emerging Roles of N(6)-Methyladenosine on HIV-1 RNA Metabolism and Viral  
649 Replication. *Frontiers in Microbiology* **9**, 576 (2018).

650 30. Abd El-Wahab, E.W. *et al.* Specific recognition of the HIV-1 genomic RNA by the  
651 Gag precursor. *Nat Commun* **5**, 4304 (2014).

652 31. Kutluay, S.B. *et al.* Global changes in the RNA binding specificity of HIV-1 gag  
653 regulate virion genesis. *Cell* **159**, 1096-1109 (2014).

654 32. Gokhale, N.S. *et al.* N6-Methyladenosine in Flaviviridae Viral RNA Genomes  
655 Regulates Infection. *Cell Host Microbe* **20**, 654-665 (2016).

656 33. Mauer, J. & Jaffrey, S.R. FTO, m(6) Am<sub>1</sub>, and the hypothesis of reversible  
657 epitranscriptomic mRNA modifications. *FEBS Lett* (2018).

658 34. Huang, Y. *et al.* Small-Molecule Targeting of Oncogenic FTO Demethylase in Acute  
659 Myeloid Leukemia. *Cancer Cell* **35**, 677-691 e610 (2019).

660 35. de Bisschop, G. *et al.* HIV-1 gRNA, a biological substrate, uncovers the potency of  
661 DDX3X biochemical activity. *Biochimie* (2019).

662 36. Karabiber, F., McGinnis, J.L., Favorov, O.V. & Weeks, K.M. QuShape: rapid,  
663 accurate, and best-practices quantification of nucleic acid probing information,  
664 resolved by capillary electrophoresis. *RNA* **19**, 63-73 (2013).

665 37. Low, J.T. & Weeks, K.M. SHAPE-directed RNA secondary structure prediction.  
666 *Methods* **52**, 150-158 (2010).

667 38. Darty, K., Denise, A. & Ponty, Y. VARNA: Interactive drawing and editing of the  
668 RNA secondary structure. *Bioinformatics* **25**, 1974-1975 (2009).

669

670 **AKNOWLEDGEMENTS**

671 Authors wish to thank Professor Cai-Guang Yang (CAS Key Laboratory of Receptor  
672 Research, Shanghai Institute of Materia Medica, Chinese Academy of Sciences) for providing  
673 MA2. Authors will also thank to Dr. Chuan He (University of Chicago), Dr. Yun-Gui Yang  
674 (Beijing Institute of Genomics, Chinese Academy of Sciences), Dr. Jin Crystal Zhao and Dr.  
675 Monica Roth (University of Wisconsin) for providing expression vectors as well as Dr. Gloria  
676 Arriagada (Universidad Andrés Bello) for providing the anti-MLV CAp30 antibody.

677

678 **FUNDING**

679 This work was funded through the FONDECYT Program (Nº 1160176 and 1190156 to RSR  
680 and 1180798 to FVE). CPM, FGdeG, SRB, BRA and PAC are recipients of a National  
681 Doctoral fellowship from CONICYT. Research at BS laboratory was funded by CNRS,  
682 Université Paris Descartes and a grant from Fondation pour la Recherche Médicale (FRM  
683 #DBI20141231337). Exchanges between RSR and BS laboratories were funded by a LIA  
684 grant from CNRS. GdB is a recipient of a fellowship from the French Ministry for  
685 "Enseignement Supérieur et Recherche".

686

687 **AUTHOR CONTRIBUTIONS**

688 CP-M designed and performed experiments, analyzed data and wrote the paper. DT-A, SR-B,  
689 BR-A, FGdeG, PA-C, CA-S, MLA and JCh performed experiments and analyzed data. CR-F  
690 performed bioinformatic analyses. GdeB performed *in vitro* experiments and analyzed data.  
691 FV-E and BS contributed to data analysis and manuscript writing. RS-R contributed to the  
692 concept and design, data analysis and manuscript writing. All the authors read and approved  
693 the final version of the manuscript.

694

695 **COMPETING FINANCIAL INTERESTS**

696 Authors declare no competing financial interests.